BOLETIN DE LA SOCIEDAD ESPAÑOLA DE
Cerámica y Vidrio
www.elsevier.es/bsecv

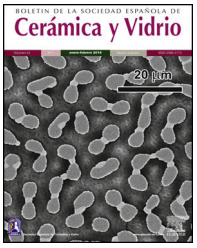

Original

The electrocatalytic oxidation of methanol using a new modified electrode based on $NiCo_2O_4$ nanoparticles incorporated into zeolite-4A

Fatemeh Ganji[a], *Khosro Mohammadi*[a,*], *Behrooz Roozbehani*[b]

[a] *Department of Chemistry, Persian Gulf University, Bushehr 75169, Iran*
[b] *Research Center of Petroleum University of Technology, Abadan, Iran*

ARTICLE INFO

Article history:
Received 24 March 2019
Accepted 1 August 2019
Available online 24 August 2019

Keywords:
Cyclic voltammetry
Chronoamperometry
Methanol
Oxidation

ABSTRACT

In this work, a new catalyst based on carbon paste (CP) modified by spinel $NiCo_2O_4$ nanoparticles and zeolite-4A was proposed and used for the electrochemical oxidation of methanol. $NiCo_2O_4$@zeolite-4A was obtained through the calcination of the physical mixture of $NiCo_2O_4$ and zeolite-4A. Their physicochemical properties were characterized by X-ray diffraction (XRD), scanning electron microscopy-energy dispersive X-ray spectra (SEM-EDS), and FT-IR techniques. The electrocatalytic performance of modified electrode based on $NiCo_2O_4$@zeolite-4A was tested using cyclic voltammetry (CV) and chronoamperomerty (CA). The result of cyclic voltammetry indicated a significant rise in the oxidation current on the surface of $NiCo_2O_4$@zeolite-4A/CPE modified electrode. The rate constant for the catalytic reaction (k) of methanol was calculated by means of a chronoamperometric technique. To sum up, the incorporation of $NiCo_2O_4$ nanoparticles into zeolite-4A provided the binary electroactive sites for catalysis of methanol oxidation as it exhibited a long-term stability for catalytic reaction, and thus a promising application.

La oxidación electrocatalítica del metanol utilizando un nuevo electrodo modificado basado en nanopartículas de $NiCo_2O_4$ incorporadas en la zeolita-4A

Palabras clave:
Voltametría cíclica
Cronoamperometría
Metanol
Oxidación

RESUMEN

En este trabajo se propuso un nuevo catalizador basado en pasta de carbono (CP) modificado por espinela de nanopartículas de $NiCo_2O_4$ y zeolita-4[a], y se utilizó para la oxidación electroquímica del metanol. Se obtuvo $NiCo_2O_4$@zeolita-4A a través de la calcinación de la mezcla física de $NiCo_2O_4$ y zeolita-4A. Sus propiedades fisicoquímicas se caracterizaron por difracción de rayos X (XRD), espectros de rayos X de barrido de energía con microscopía electrónica

* *Corresponding author.*
E-mail address: khmohammadi@pgu.ac.ir (K. Mohammadi).
https://doi.org/10.1016/j.bsecv.2019.08.003

de barrido (SEM-EDS) y técnicas de FT-IR. El rendimiento electrocatalítico del electrodo modificado basado en $NiCo_2O_4$@zeolita-4A se probó utilizando la voltametría cíclica (CV) y cronoamperometría (CA). El resultado de la voltametría cíclica indicó un aumento significativo de la corriente de oxidación en la superficie del electrodo modificado con zeolita-4A/CPE de $NiCo_2O_4$. La constante de velocidad para la reacción catalítica (k) del metanol se calculó mediante una técnica cronoamperométrica. En resumen, la incorporación de nanopartículas de $NiCo_2O_4$ en la zeolita-4A proporcionó los sitios electroactivos binarios para la catálisis de la oxidación de metanol, ya que exhibió una estabilidad a largo plazo para la reacción catalítica y, por lo tanto, una aplicación prometedora.

Introduction

Fuel cells (FCs) are among the most common technologies in energy storage. They prove to be environmentally friendly and highly efficient in solving the energy problems of the modern world [1]. Although hydrogen is currently the predominant fuel as, by way of example, fuel cell vehicles under commercial development all use hydrogen fuel, methanol could be a promising alternative owing to its simplicity of operation, transportation and storage [2]. The most commonly used electrodes in direct methanol fuel cell (DMFC), however, exhibit low kinetic and high overpotential. Likewise, Pt-based metal, bimetal and their alloys such as Pt, Pt-Ru, Pt-Fe-Ru are also known to be the best catalysts in investigating the mechanism and kinetic of electrocatalytic oxidation of methanol [3–9] as they are very active in the oxidation of methanol. But these catalysts are expensive and have low natural abundance. Therefore, there is a need to develop alternative low-cost transition metal oxides based catalysts that could overcome these drawbacks.

Transition metal oxides are utilized in heterogeneous catalysis and electrocatalysis by virtue of their intrinsic redox and tunable chemical, morphological, and textural properties, which can be rigidly bound on the substrate materials, i.e., nanoporous architectures with high surface areas and pore volumes [10–12]. Several substrate materials such as carbon nanotube, graphene oxide, and mesoporous silica have been hitherto exploited to improve electro-catalytic activity of metal species [13–17]. The ordered mesoporous materials with high surface area and porous nature known as zeolites are not only among the most commonly used nanoporous supports and substrate but also considered among the best solutions to overcome the pitfalls of catalytic oxidation of alcohol for fuel cells [18]. It should be noted that zeolite comes in different types, of which zeolite-4A is the most widely studied and employed framework, functioning as a substrate for different catalytic reactions [10–24].

Similarly, spinel crystal structure of the type AB_2O_4 has been used in a broad range of disciplines, from electrochemistry, through catalysis to electronics. In a normal spinel, the A cations occupy the tetrahedral sites while the B cations fill the octahedral sites in the cubic closed packing formed by the anions O^{2-}. In an inverse spinel structure, in contrast, part of the B cations occupy the tetrahedral sites, possibly distorting the lattice by their size, while the A cations fill the octahedral sites [24–26]. One of the binary metal oxides known as $NiCo_2O_4$ adopts an inverse spinel structure in which nickel ions fill the octahedral sites whereas cobalt ions are scattered across the tetrahedral and octahedral sites of the structure. $NiCo_2O_4$ demonstrates higher electronic conductivity and electrochemical activity than those of nickel and cobalt oxides and hence higher redox chemistry than each single component [27–30]. That being so, $NiCo_2O_4$ has been utilized in such diverse fields as magnetic materials, electro-catalysts, optical limiters and switches, chemical sensors, and lithium ion batteries [31].

In the present research, nickel cobaltite nanoparticles ($NiCo_2O_4$ NPs) was synthesized via a facile hydrothermal method in the presence of urea and $NiCo_2O_4$ nanoparticles were incorporated into the zeolite-4A. In the end, electrocatalytic behavior of $NiCo_2O_4$@zeolite-4A modified electrode toward methanol oxidation was observed using the cyclic voltammetry and chronoamperomerty in a conventional three-electrode electrochemical setup. The finding of this study indicated that the electrode modified by $NiCo_2O_4$@zeolite-4A might be more efficient in the oxidation of methanol than other catalysts.

Experimental

Materials

All chemicals used in this study were of analytical grade and utilized as received without undergoing any further purification. Sodium aluminate, Cetyl Trimethyl Ammonium Bromide (CTAB), NaOH pellets and Tetraethylorthosilicate (TEOS) were purchased from Sigma–Aldrich; and urea, cobalt (II) chloride hexahydrate and nickel (II) chloride hexahydrate were obtained from Merck.

Synthesis of zeolite-4A, $NiCo_2O_4$ and $NiCo_2O_4$@zeolite-4A

Zeolite-4A was prepared using a formerly reported method [32]. That is to say, 4 g of NaOH pellets and approximately half of the required amount of CTAB were dissolved in deionized water, in which 8 g of sodium aluminate was added later. The resulting mixture was stirred until a clear solution was formed (solution A). 15.6 g of TEOS was added to the rest of

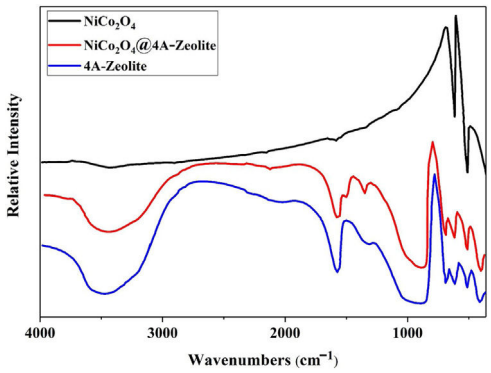

Fig. 1 – FT-IR of $NiCo_2O_4$, zeolite-4A and $NiCo_2O_4$@zeolite-4A.

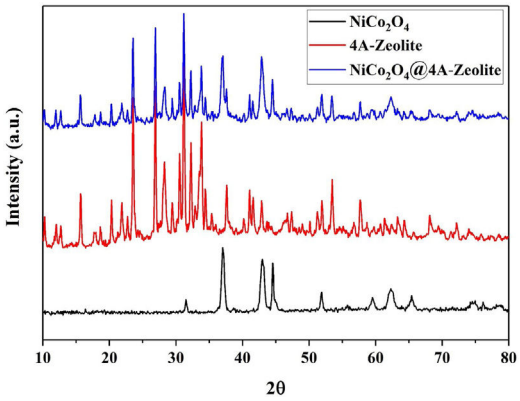

Fig. 2 – XRD pattern of $NiCo_2O_4$, zeolite-4A and $NiCo_2O_4$@zeolite-4A.

the required amount of CTAB solution. After 2 h of continuous stirring, a homogeneous and clear solution was created (solution B). A blend of solutions A and B formed the initial clear solution for synthesis which was then crystallized hydrothermally at 100 °C for 24 h in a stainless-steel autoclave. Next, the precipitation product was filtered and washed using deionized water. The final product was eventually dried in a vacuum oven at 60 °C, and later calcined at 550 °C.

$NiCo_2O_4$ was synthesized in a similar way [33]. Namely, 10 mmol $CoCl_2{\cdot}6H_2O$, 5 mmol $NiCl_2{\cdot}6H_2O$ and 50 mmol urea were dissolved in 70 mL deionized water and stirred until a bright pink colored solution was formed. The mixture was then transferred into a Teflon-lined stainless-steel autoclave, and hydrothermally treated at 120 °C for 6 h. Autoclave was already cooled at room temperature while the reaction mixture was filtered and washed with distilled water and ethanol. The material was later calcined at 300 °C for 4 h. In the end, $NiCo_2O_4$ and zeolite-4A with weight ratio 40 to 60, denoted as $NiCo_2O_4$ (40%)/zeolite-4A were grounded uniformly with ethanol using mortar and pastel. Ethanol was slowly removed during the mixing process. The mixture was then heated at 473 K in air for 45 min to remove the residual ethanol followed by calcination at 613 K for 12 h.

Results

The FT-IR spectra of samples are given in Fig. 1. The FT-IR spectra of pristine $NiCo_2O_4$ spectrum showed two strong peaks at 557 and 652 cm^{-1}, referring to the stretching vibrations of the Ni–O and Co–O bonds in nickel cobalt oxide, respectively [30]. Given the high degree of hydration, the FT-IR spectra of pure zeolite-4A and $NiCo_2O_4$@zeolite-4A exhibited a broad peak around 3400 cm^{-1}, indicating the presence of hydroxyl groups. All absorption peaks around 450–1000 cm^{-1} alluded to metal–oxygen bonds, owing to the existence of metal complexes or metal oxide nanoparticles brought about by low concentrations of metal loaded on the zeolite-4A. The comparison between FT-IR spectrum of $NiCo_2O_4$@zeolite-4A and the pure zeolite-4A spectrum revealed that the original zeolite spectrum about 973 cm^{-1} ((Si, Al)–O) appeared in lower region. This peak shifted 5 cm^{-1} and appeared in 968 cm^{-1} which could be caused by the interaction between zeolite network and nickel cobalt oxide nanoparticles [34–37].

The X-ray diffraction (XRD) pattern of all samples are shown in Fig. 2. As depicted in XRD, all the diffraction peaks for $NiCo_2O_4$ and the space groups Fd-3m corresponded to the standard patterns of the spinel $NiCo_2O_4$ phase (JCPDS card No. 73-1702) and all the diffraction peaks of zeolite-4A with the space groups Fm-3c were, likewise, confirmed by (JCPDS card No. 39-222). Diffraction peaks of $NiCo_2O_4$ NPs were observed at XRD pattern of zeolite-4A after loading $NiCo_2O_4$ NPs on zeolite-4A, which indicated that $NiCo_2O_4$ NPs were well loaded into zeolite-4A.

Fig. 3 illustrates SEM images of $NiCo_2O_4$, zeolite-4A and $NiCo_2O_4$@zeolite-4A. As can be seen, the $NiCo_2O_4$ nanoparticles were composed of uniform flower-like structures whose average size is 1.6 μm in diameter. These 3D flower-like structures were assembled by a large number of nanosheets with an average thickness of 16 nm (Fig. 3a and b). Fig. 3c and d indicates that $NiCo_2O_4$@zeolite-4A had the spherical structure with particle diameter ranging from 46.2 nm to 57 nm. The comparison between Fig. 3c, d and e revealed that the cubic structure morphology of zeolite transformed into a spherical structure subsequent to the loading of $NiCo_2O_4$ nanoparticles.

It can be inferred from the EDX analysis that the obtained $NiCo_2O_4$@zeolite-4A (Fig. 3f) had the purity of the samples containing only Si, Al, O, Na, Ni and Co elements. The loading of $NiCo_2O_4$ nanoparticles to the zeolite-4A had already been shown in Fig. 3c.

Preparation of the working electrodes

Electrochemical measurements were carried out by means of a Sama-500 electrochemical workstation while the electrocatalytic performance was tested using cyclic voltammetry (CV) and chronoamperometry (CA). All the measurements were performed in a conventional three-electrode system containing Ag/AgCl as the reference electrode (3 M KCl) a platinum wire (both from Azar Electrode Co., Iran) as the counter electrode and $NiCo_2O_4$ modified carbon paste electrode (CPE) as the working electrode. The $NiCo_2O_4$@zeolite-4A and zeolite-4A modified carbon paste electrode were prepared by mixing

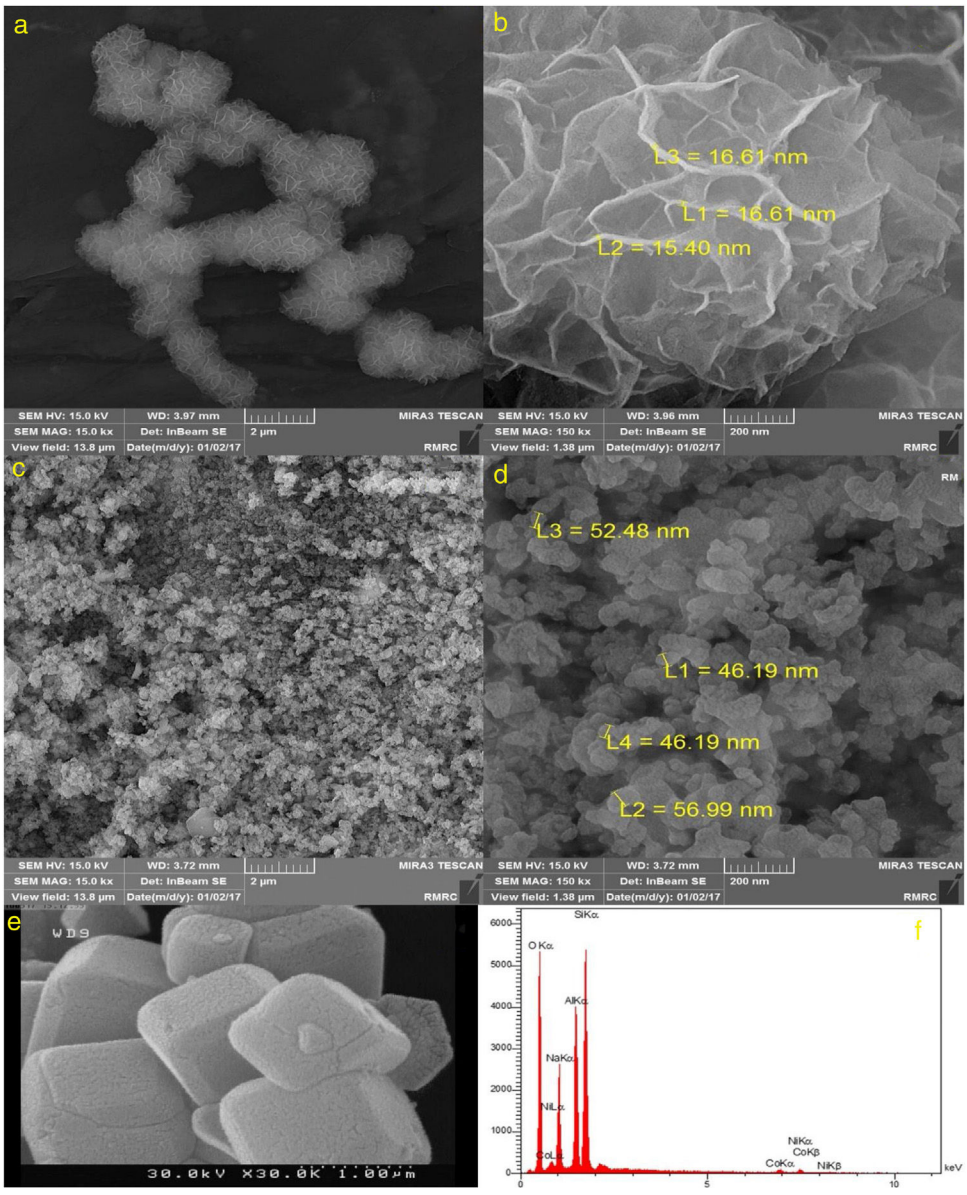

Fig. 3 – SEM images of $NiCo_2O_4$ (a, b), $NiCo_2O_4$@zeolite-4A (c, d), zeolite-4A (e) and EDX spectra of $NiCo_2O_4$@zeolite-4A (f).

$NiCo_2O_4$@zeolite-4A and zeolite-4A in a ratio of 30:70% (w/w) with the graphite powder and then with diethyl ether. After solvent evaporation, paraffin was blended by hand in a mortar, the resulting paste of which was inserted in the bottom of a glass tube (with internal radius 1.5 mm). The electrical connection was implemented by a Cu wire. The unmodified CPE were produced in a similar manner, except for the addition of an appropriate amount of $NiCo_2O_4$ to the graphite powder. The electrodes were ultimately polished on a very fine smooth paper.

Electrochemical behavior of modified electrode

The electrochemical behaviors of different modified electrodes were examined by cyclic voltammetry recorded at a potential sweep rate of 25 mV s^{-1} for methanol oxidation (Fig. 4). As shown in Fig. 4, $NiCo_2O_4$@zeolite-4A/CPE displayed large oxidation current with the oxidation peak current of 60 μA (curve a). On the surface of zeolite-4A/CPE and CPE (curve c, d), however, no redox peaks were observed under the same condition. It can be inferred from Fig. 4c and d that the zeolite-4A played no significant role in the oxidation of methanol. The oxidation peak current on the surface of $NiCo_2O_4$/CPE was 28 μA (curve b) which proved that the presence of $NiCo_2O_4$ in CPE could increase methanol oxidation peak currents. The findings revealed that the presence of synthesized $NiCo_2O_4$ nanoparticles and zeolite-4A on $NiCo_2O_4$@zeolite-4A/CPE surface were significantly improved by virtue of electrochemical oxidation response of methanol.

Fig. 5a displays the cyclic voltammetry behavior of the $NiCo_2O_4$@zeolite-4A/CPE toward the methanol concentrations in the range of 0–0.6 V at the scan rate of 25 mV s^{-1}. The concentration of methanol changed from 0 to 0.5 M in 0.1 M NaOH solution. As evident in Fig. 5, the amount of electrocatalytic

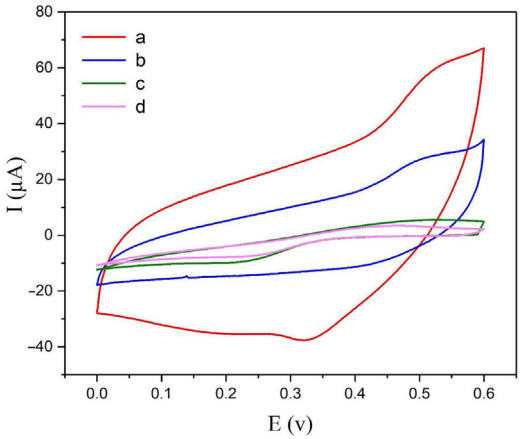

Fig. 4 – Cyclic voltammogram recorded on (a) $NiCo_2O_4$@zeolite-4A/CPE, (b) $NiCo_2O_4$/CPE, (c) zeolite-4A/CPE and (d) CPE in the presence of 0.5 M methanol in 0.1 M NaOH at scan rate of 25 mV s^{-1}.

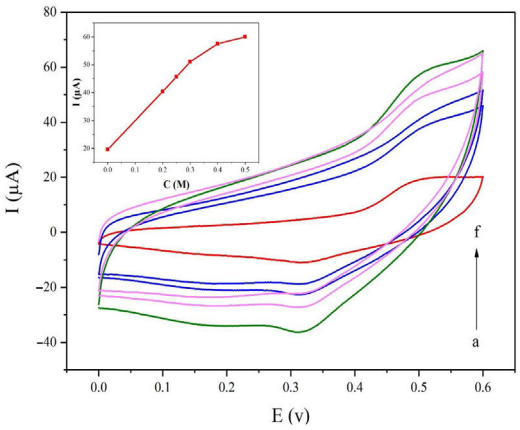

Fig. 5 – Cyclic voltammograms of the $NiCo_2O_4$@zeolite-4A/CPE at the scan rate of 25 mV s^{-1} with different concentrations of methanol: (a) 0.0, (b) 0.2, (c) 0.25, (d) 0.3, (e) 0.4, and (f) 0.5 M, respectively in 0.1 M NaOH. Inset shows plot of I_{pa} vs. $\nu^{1/2}$ for the oxidation of methanol on $NiCo_2O_4$@zeolite-4A/CPE.

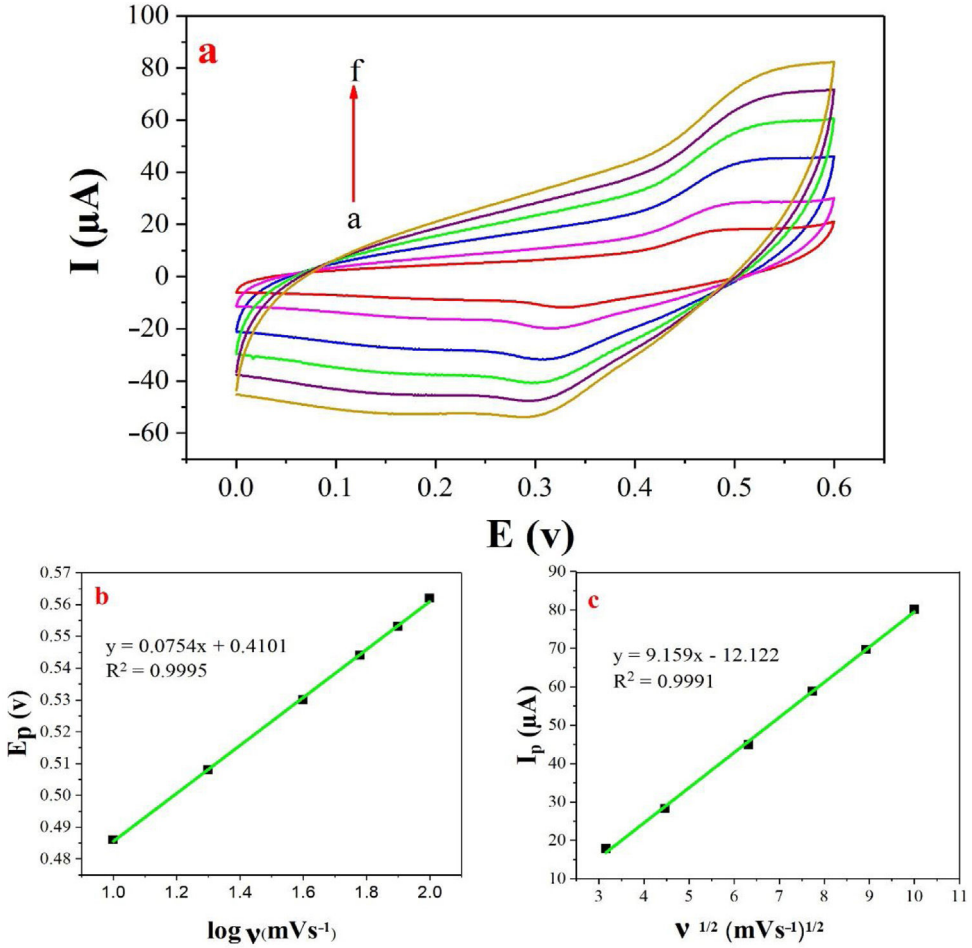

Fig. 6 – (a) Cyclic voltammograms of the $NiCo_2O_4$@zeolite-4A/CPE in the presence of 0.1 M methanol, at different scan rates of (a) 10, (b) 20, (c) 40, (d) 60, (e) 80 and (f) 100 mV s^{-1} in 0.1 M NaOH. (b) and (c) Plot of E_p vs. log ν and I_{pa} vs. $\nu^{1/2}$ for the oxidation of methanol on $NiCo_2O_4$@zeolite-4A/CPE.

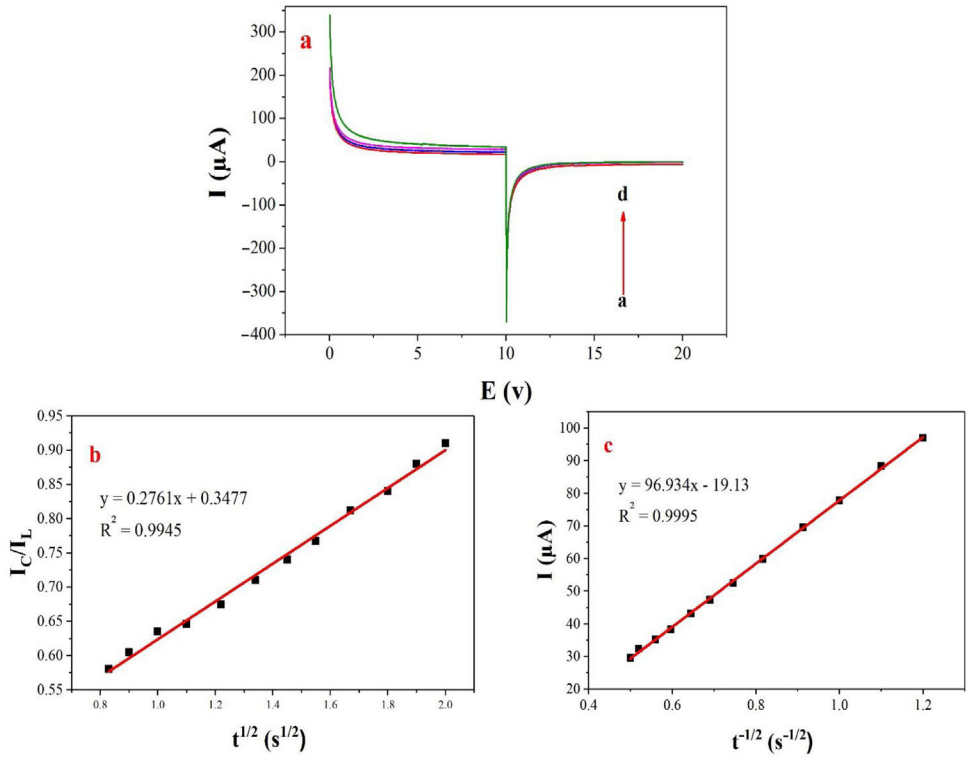

Fig. 7 – (a) Chronoamperograms obtained at the $NiCo_2O_4$@zeolite-4A/CPE in absence (a) and presence of (b) 0.05, (c) 0.1, and (d) 0.2 M of methanol, first and second potential steps were 0.52 and 0.32 V vs. Ag–AgCl, respectively, in 0.1 M NaOH solution. (b) Dependence of current on $t^{-1/2}$, derived from the data of chronoamperograms. (c) Dependence of I_C/I_L on $t^{1/2}$ derived from the data of chronoamperogams of in the main panel.

current increased after adding the concentration of methanol until 0.5 M which confirmed the excellent electrocatalytic behavior of $NiCo_2O_4$@zeolite-4A/CPE.

The examination of scan rate can shed more light on electrochemical mechanisms and kinetic characteristics of methanol. Fig. 6a depicts the cyclic voltammograms of methanol on $NiCo_2O_4$@zeolite-4A/CPE in 0.1 M NaOH between 0 and 0.6 V at various scan rates. As can be seen in Fig. 6c, the anodic oxidation current (I_p) increased linearly proportional to the square roots of scan rates from 10 to 100 mV s^{-1} indicating a probable occurrence of a diffusion-controlled process in the oxidation of methanol on $NiCo_2O_4$@zeolite-4A/CPE. To obtain further information on the rate determining step, a Tafel plot was developed for the methanol on the surface of $NiCo_2O_4$@zeolite-4A/CPE using the data derived from the raising part of the log ν–voltage curve (Fig. 6b). The slope of the Tafel plot is equal to $n(1-\alpha)F/2.3RT$ and α is 0.59.

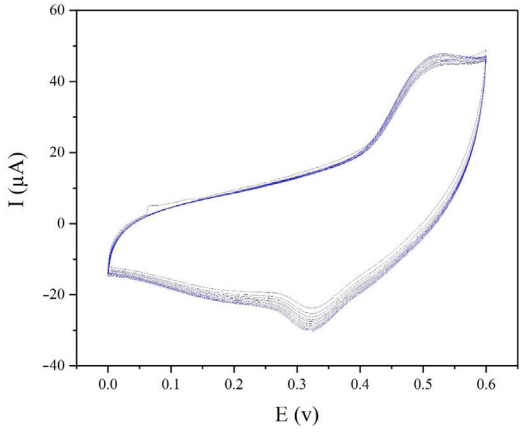

Fig. 8 – Successive cyclic voltammograms (50th cycles) of $NiCo_2O_4$@zeolite-4A/CPE in 0.1 M NaOH and 0.5 M methanol solution. Scan rate 25 mV s^{-1}.

Chronoamperometric studies

Double potential step chronoamperometry along with some other electrochemical methods were used to examine the catalytic rate constant of the methanol oxidation on the $NiCo_2O_4$@zeolite-4A/CPE. As depicted in Fig. 7, the current–time profiles recorded by setting the potential of modified electrode at 520 mV (in first step) and 320 mV (in second step) vs. Ag/AgCl (KCl 3 M) were determined based on peak potential of redox process at various concentrations of methanol. The plot of I vs. $t^{-1/2}$ showed a linear dependence in the absence of methanol (Fig. 7c). From exponential I–t amperograms (Fig. 7a) a diffusion controlled process occurs which can be modeled by a Cottrell equation [38]. From chronoamperograms, the rate constant for the chemical reaction between the methanol and redox sites of $NiCo_2O_4$@zeolite-4A/CPE

modified electrode can be evaluated according to following equation [39]:

$$\frac{I_C}{I_L} = \gamma^{1/2}[\pi^{1/2} erf(\gamma^{1/2}) + \exp(-\gamma)\gamma^{1/2}] \quad (1)$$

where I_C is the catalytic current of $NiCo_2O_4$@zeolite-4A/CPE in the presence of methanol, I_L is limiting current in the absence of methanol and $\gamma = kC_0t$ (C is the argument of error function). C_0 in the argument refers to the concentration of methanol in bulk solution. When γ is more than 2, the error function is almost equal to 1 and the above equation can be summarized as follows:

$$\frac{I_C}{I_L} = \gamma^{1/2}\pi^{1/2} = \pi^{1/2}(\kappa C_0 t)^{1/2} \quad (2)$$

where k, C_0 and t are the catalytic rate constant ($cm^3\,mol^{-1}\,s^{-1}$), methanol concentration ($mol\,cm^{-3}$) and time passed (s), respectively. From the slope linear plot of I_C/I_L vs. $t^{1/2}$ obtained from the plot of chronoamperogram of $NiCo_2O_4$@zeolite-4A/CPE, the value of k for a given concentration of substrate can be easily calculated. Fig. 7b displays one such plot, constructed from the chronoamperogram of the $NiCo_2O_4$@zeolite-4A/CPE in the absence and presence of 0.05 M methanol. The mean value of k was found to be approximately $1.1 \times 10^3\,cm^3\,mol^{-1}\,s^{-1}$. From Eq. (2), the findings confirmed that $NiCo_2O_4$@zeolite-4A/CPE represents a good catalytic activity toward the methanol oxidation.

Stability of $NiCo_2O_4$@zeolite-4A/CPE

The electrochemical stability of the modified electrode is also a very important factor to be evaluated. In order to investigate the stability of modified electrode, cyclic voltammograms of modified electrode were recorded in presence of 0.1 M methanol (Fig. 8). As seen in Fig. 8, the CV plots are quite stable and the current density at 0.55 V (vs. Hg/HgO) exhibits 95% retention after 50 cycles at 25 mV s^{-1}.

Conclusion

In this study, spinel $NiCo_2O_4$ nanoparticles and zeolite-4A were prepared via a facile hydrothermal route. The findings of SEM and XRD revealed that $NiCo_2O_4$ nanoparticles of the flower-like 3D structures were assembled by a large number of nanosheets with an average thickness of 16 nm while zeolite-4A had the spherical structure with particle diameter ranging from 46.2 nm to 57 nm. The behavior of modified electrode in electrocatalytic process of methanol oxidation was investigated using cyclic voltammetry and chronoamperometry. From cyclic voltammetry, the modified electrode delivered an anodic oxidation current about 60 μA at 0.6 V in 1 M KOH and 0.5 M methanol and displayed a good stability with 95% current retention after 50 cycles at 30 mV s^{-1}. The modified electrode could enhance the electro-catalytic oxidation and overcome the low kinetic of reaction of methanol due to its rich binary electro-active sites of Ni and Co species, high intrinsic electron conductivity and superior surface structures.

REFERENCES

[1] S. Basri, S.K. Kamarudin, Process system engineering in direct methanol fuel cell, Int. J. Hydrogen Energy 36 (2011) 6219–6236.
[2] Y.B. He, G.R. Li, Z.L. Wang, Y.N. Ou, Y.X. Tong, Pt nanorods aggregates with enhanced electrocatalytic activity toward methanol oxidation, J. Phys. Chem. C 114 (2010) 19175–19181.
[3] D.H. Lin, Y.X. Jiang, S.R. Chen, S.P. Chen, S.G. Sun, Preparation of Pt nanoparticles supported on ordered mesoporous carbon FDU-15 for electrocatalytic oxidation of CO and methanol, Electrochim. Acta 67 (2012) 127–132.
[4] C.H. Lee, C.W. Lee, D.I. Kim, S.E. Bae, Characteristics of methanol oxidation on Pt–Ru catalysts supported by HOPG in sulfuric acid, Int. J. Hydrogen Energy 27 (2002) 445–450.
[5] H. Wang, C. Wingender, H. Baltruschat, M. Lopez, M.T. Reetz, Methanol oxidation on Pt, PtRu, and colloidal Pt electrocatalysts: a DEMS study of product formation, J. Electroanal. Chem. 509 (2001) 163–169.
[6] B. Habibi, M.H. Pournaghi-Azar, H. Abdolmohammad-Zadeh, H. Razmi, Electrocatalytic oxidation of methanol on mono and bimetallic composite films: Pt and Pt–M (M = Ru, Ir and Sn) nano-particles in poly (o-aminophenol), Int. J. Hydrogen Energy 34 (2009) 2880–2892.
[7] C.K. Poh, Z. Tian, J. Gao, Z. Liu, J. Lin, Y.P. Feng, F. Su, Nanostructured trimetallic Pt/FeRuC, Pt/NiRuC, and Pt/CoRuC catalysts for methanol electrooxidation, J. Mater. Chem. 22 (2012) 13643–13652.
[8] D. Xiang, L. Yin, Well-dispersed and size-tuned bimetallic PtFe x nanoparticle catalysts supported on ordered mesoporous carbon for enhanced electrocatalytic activity in direct methanol fuel cells, J. Mater. Chem. 22 (2012) 9584–9593.
[9] B. Habibi, M.H. Pournaghi-Azar, Methanol oxidation on the polymer coated and polymer-stabilized Pt nano-particles: a comparative study of permeability and catalyst particle distribution ability of the PANI and its derivatives, Int. J. Hydrogen Energy 35 (2010) 9318–9328.
[10] A. Cao, R. Lu, G. Veser, Stabilizing metal nanoparticles for heterogeneous catalysis, PCCP 12 (2010) 13499–13510.
[11] D. Astruc, F. Lu, J.R. Aranzaes, Nanoparticles as recyclable catalysts: the frontier between homogeneous and heterogeneous catalysis, Angew. Chem. Int. Ed. 44 (2005) 7852–7872.
[12] T.L. Cui, W.Y. Ke, W.B. Zhang, H.H. Wang, X.H. Li, J.S. Chen, Encapsulating palladium nanoparticles inside mesoporous MFI zeolite nanocrystals for shape-selective catalysis, Angew. Chem. 128 (2016) 9324–9328.
[13] S. Abouali, M.A. Garakani, Z.-L. Xu, J.-K. Kim, $NiCo_2O_4$/CNT nanocomposites as bi-functional electrodes for Li ion batteries and supercapacitors, Carbon 102 (2016) 262–272.
[14] M. Ho, P. Khiew, D. Isa, T. Tan, W. Chiu, C.H. Chia, A review of metal oxide composite electrode materials for electrochemical capacitors, Nano 9 (2014) 1430002.
[15] H. Rong, Y. Qin, Z. Jiang, Z.-J. Jiang, M. Liu, A novel $NiCo_2O_4$@GO hybrid composite with core–shell structure as high-performance anodes for lithium-ion batteries, J. Alloys Compd. 731 (2018) 1095–1102.
[16] E. Mitchell, A. Jimenez, R.K. Gupta, B.K. Gupta, K. Ramasamy, M. Shahabuddin, et al., Ultrathin porous hierarchically textured $NiCo_2O_4$–graphene oxide flexible nanosheets for high-performance supercapacitors, New J. Chem. 39 (2015) 2181–2187.
[17] C. Zhen, X. Zhang, W. Wei, W. Guo, A. Pant, X. Xu, et al., Nanostructural origin of semiconductivity and large magnetoresistance in epitaxial $NiCo_2O_4/Al_2O_3$ thin films, J. Phys. D: Appl. Phys. 51 (2018) 145308.

[18] M. Abrishamkar, A. Izadi, Nano-ZSM-5 zeolite: synthesis and application to electrocatalytic oxidation of ethanol, Micropor. Mesopor. Mater. 180 (2013) 56–60.
[19] L. Wang, S. Xu, S. He, F.-S. Xiao, Rational construction of metal nanoparticles fixed in zeolite crystals as highly efficient heterogeneous catalysts, Nano Today 20 (2018) 74–83, http://dx.doi.org/10.1016/j.nantod.2018.04.004.
[20] S.M. Auerbach, K.A. Carrado, P.K. Dutta, Handbook of Zeolite Science and Technology, CRC Press, 2003.
[21] F. Liu, B.-R. Ma, D. Zhou, Xiang Y-h, L-x. Xue, Breaking through tradeoff of polysulfone ultrafiltration membranes by zeolite 4A, Micropor. Mesopor. Mater. 186 (2014) 113.
[22] S.S. Bukhari, J. Behin, H. Kazemian, S. Rohani, Conversion of coal fly ash to zeolite utilizing microwave and ultrasound energies: a review, Fuel 140 (2015) 250–266.
[23] N.L. Torad, M. Naito, J. Tatami, A. Endo, S.Y. Leo, S. Ishihara, et al., Highly crystallized nanometer-sized zeolite a with large Cs adsorption capability for the decontamination of water, Chem-Asian J. 9 (2014) 759–763.
[24] Y.P. De Peña, W. Rondón, Linde type a zeolite and type Y faujasite as a solid-phase for lead, cadmium, nickel and cobalt preconcentration and determination using a flow injection system coupled to flame atomic absorption spectrometry, Am. J. Analyt. Chem. 4 (2013) 387.
[25] F.O. Ernst, H.K. Kammler, A. Roessler, S.E. Pratsinis, W.J. Stark, J. Ufheil, et al., Electrochemically active flame-made nanosized spinels: $LiMn_2O_4$, $Li_4Ti_5O_{12}$ and $LiFe_5O_8$, Mater. Chem. Phys. 101 (2007) 372–378.
[26] X. Zeng, J. Zhang, S. Zhu, X. Deng, H. Ma, J. Zhang, et al., Direct observation of cation distributions of ideal inverse spinel $CoFe_2O_4$ nanofibres and correlated magnetic properties, Nanoscale 9 (2017) 7493–7500.
[27] M. Huš, V.D. Dasireddy, N.S. Štefančič, B. Likozar, Mechanism, kinetics and thermodynamics of carbon dioxide hydrogenation to methanol on $Cu/ZnAl_2O_4$ spinel-type heterogeneous catalysts, Appl. Catal. B: Environ. 207 (2017) 267–278.
[28] U.T. Nakate, S. Kale, Microwave assisted synthesis and characterizations of $NiCo_2O_4$ nanoplates and electrical, magnetic properties, Mater. Today 3 (2016) 1992–1998.
[29] V. Venkatachalam, A. Alsalme, A. Alghamdi, R. Jayavel, Hexagonal-like $NiCo_2O_4$ nanostructure based high-performance supercapacitor electrodes, Ionics 23 (2017) 977–984.
[30] M.A. Prathap, R. Srivastava, Synthesis of $NiCo_2O_4$ and its application in the electrocatalytic oxidation of methanol, Nano Energy 2 (2013) 1046–1053.
[31] D.P. Dubal, P. Gomez-Romero, B.R. Sankapal, R. Holze, Nickel cobaltite as an emerging material for supercapacitors: an overview, Nano Energy 11 (2015) 377–399.
[32] R. Ding, L. Qi, H. Wang, A facile and cost-effective synthesis of mesoporous $NiCo_2O_4$ nanoparticles and their capacitive behavior in electrochemical capacitors, J. Solid State Electrochem. 16 (2012) 3621–3633.
[33] Y.C. Feng, Y. Meng, F.X. Li, Z.P. Lv, J.W. Xue, Synthesis of mesoporous LTA zeolites with large BET areas, J. Porous Mater. 20 (2013) 465–471.
[34] E. Umeshbabu, G. Rajeshkhanna, P. Justin, G.R. Rao, Synthesis of mesoporous $NiCo_2O_4$–rGO by a solvothermal method for charge storage applications, RSC Adv. 5 (2015) 66657–66666.
[35] R. Belaabed, S. Elabed, A. Addaou, A. Laajab, M.A. Rodríguez, A. Lahsini, Synthesis of LTA zeolite for bacterial adhesion, Bol. Soc. Esp. Cerám. V 55 (2016) 152–158.
[36] C.A. Rios, C.D. Williams, M.A. Fullen, Nucleation and growth history of zeolite LTA synthesized from kaolinite by two different methods, Appl. Clay Sci. 42 (2009) 446–454.
[37] R.S. Razavi, M.R. Loghman-Estarki, Synthesis and characterizations of copper oxide nanoparticles within zeolite Y, J. Clust. Sci. 23 (2012) 1097–1106.
[38] D. Ghanbari, S. Sharifi, A. Naraghi, G. Nabiyouni, Photo-degradation of azo-dyes by applicable magnetic zeolite Y–silver–$CoFe_2O_4$ nanocomposites, J. Mater. Sci.: Mater. Electron. 27 (2016) 5315–5323.
[39] A.J. Bard, L.R. Faulkner, Electrochemical Methods, Fundamentals and Applications, Wiley; John and Sons, New York, 2001.